Inorganic Chemistry

Article

pubs.acs.org/IC

# Synthesis and Characterization of $CuAlO_2$ and $AgAlO_2$ Delafossite Oxides through Low-Temperature Hydrothermal Methods

Dehua Xiong,[†,‡] Xianwei Zeng,[†] Wenjun Zhang,[†] Huan Wang,[†] Xiujian Zhao,[‡] Wei Chen,*[,†] and Yi-Bing Cheng[†,§]

[†]Michael Grätzel Centre for Mesoscopic Solar Cells, Wuhan National Laboratory for Optoelectronics and College of Optoelectronic Science and Engineering, Huazhong University of Science and Technology, Wuhan 430074, People's Republic of China

[‡]State Key Laboratory of Silicate Materials for Architectures, Wuhan University of Technology, Wuhan 430070, People's Republic of China

[§]Department of Materials Engineering, Monash University, Melbourne, Victoria, 3800, Australia

**ABSTRACT:** In this work, we present one-step low temperature hydrothermal synthesis of submicrometer particulate $CuAlO_2$ and $AgAlO_2$ delafossite oxides, which are two important *p*-type transparent conducting oxides. The synthesis parameters that affect the crystal formation processes and the product morphologies, including the selection of starting materials and their molar ratios, the pH value of precursors, the hydrothermal temperature, pressure, and reaction time, have been studied. $CuAlO_2$ crystals have been synthesized from the starting materials of CuCl and $NaAlO_2$ at 320−400 °C, and from $Cu_2O$ and $Al_2O_3$ at 340−400 °C, respectively. $AgAlO_2$ crystals have been successfully synthesized at the low temperature of 190 °C, using $AgNO_3$ and $Al(NO_3)_3$ as the starting materials and NaOH as the mineralizer. The detailed elemental compositions, thermal stability, optical properties, and synthesis mechanisms of $CuAlO_2$ and $AgAlO_2$ also have been studied. Noteworthy is the fact that both $CuAlO_2$ and $AgAlO_2$ can be stabilized up to 800 °C, and their optical transparency can reach 60%−85% in the visible range. Besides, it is believed the crystal formation mechanisms uncovered in the synthesis of $CuAlO_2$ and $AgAlO_2$ will prove insightful guidlines for the preparation of other delafossite oxides.

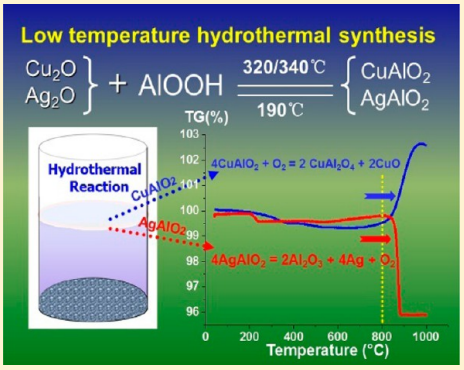


## 1. INTRODUCTION

Since the first discovery of *p*-type transparent conductivity of $CuAlO_2$ films with delafossite structure by Kawazoe et al. in 1997,[1] many studies have been carried out to develop relevant novel $AMO_2$ *p*-type semiconductors. To date, numerous $AMO_2$ compounds (where A = Ag, Cu; and M = B, Al, Ga, In, Fe, Cr, Sc, Y, etc.) have been reported with high *p*-type conductivity ($10^{-2}$−$10^2$ S $cm^{-1}$) and high optical transparency (50%−85%), dependent on their chemical compositions and film deposition methods.[1−9] These delafossite oxides could play important roles in diverse photoelectronic and photoelectrochemical applications, such as field electron emitters, light-emitting diodes, solar cells, functional windows, photocatalysts, and so on.[9−20]

Various methods for preparing delafossite oxides have been investigated such as high-temperature solid-state reactions,[21,22] cation exchange reactions,[23,24] hydrothermal reactions[5−7,15−17] for the powders synthesis, and sputtering,[25,26] sol−gel,[27,28] pulsed laser deposition (PLD)[29,30] for the preparation of thin films. Since target material for thin film deposition is composed of particles, the synthesis of phase-pure powder is the required initial step. Some general rules leading to the formation of $AMO_2$ oxides could be found in diverse synthesis methods. For example, copper-based delafossite oxides ($CuAlO_2$, $CuCrO_2$, $CuFeO_2$, $CuScO_2$) could be synthesized readily via high-temperature solid-state reactions under an inert atmosphere ($N_2$ or Ar) at ∼800−1200 °C, since $Cu^+$ is even more stable than $Cu^{2+}$ at high temperatures.[8,12,21,22] However, for the low-temperature hydrothermal synthesis of $CuAlO_2$, $CuCrO_2$, and $CuGaO_2$, the raised difficulty rests with how to reduce the soluble $Cu^{2+}$ precursor to $Cu^+$ and maintain the valence of $Cu^+$ in the monovalent state in a wet chemical environment.[4] For the synthesis of silver-based delafossite oxides, solid-state reactions at high temperature generally encountered practical problems, because of the easy decomposition of $Ag_2O$ to elemental silver at a temperature of ∼300 °C. Therefore, most reported silver-based delafossite oxides, such as $AgInO_2$, $AgCrO_2$, $AgAlO_2$, and $AgGaO_2$, were synthesized via low-temperature hydrothermal methods in closed reaction systems.[5,23,24,31−33] Moreover, among the various delafossite oxides, $CuAlO_2$ and $AgAlO_2$ are more difficult to synthesize, because of the higher crystal formation energy barrier, which is associated with cleavage and reorganization of the high-energy Al−O bonds. Conversely, these two aluminum-based delafossite oxides are superior in chemical and thermal stability than other delafossite oxides; besides, high optical transparency and a low-cost aluminum source are two other important

**Received:** January 14, 2014
**Published:** April 4, 2014

   dx.doi.org/10.1021/ic500090g | *Inorg. Chem.* 2014, 53, 4106−4116

advantages of these two materials, which are highly desired in many practical applications. Although the synthesis of $CuAlO_2$ nanocrystals at 400 °C via supercritical hydrothermal methods has been reported since 2004,[3] few reports have followed up such a procedure, which might be hard to reproduce. Besides, until now, there have been few systematical studies focusing on the hydrothermal synthesis mechanism of aluminum-based delafossite oxides. This work, which is the first to elucidate the effects of the critical hydrothermal synthesis parameters, is of great significance.

Systematic studies have been carried out to prepare phase-pure $CuAlO_2$ and $AgAlO_2$. The effects of the various synthesis parameters on the crystal formation, including the selection on the starting materials and their molar ratios, the pH value of precursors, hydrothermal temperature, pressure and reaction time, have been identified. The synthesis of delafossite oxide crystals of $CuAlO_2$ and $AgAlO_2$ have been successfully expanded to a lower temperature range, which is 320 °C for the $CuAlO_2$ and 190 °C for the $AgAlO_2$, respectively. The crystal phases and morphologies, compositions, and chemical states of elements, thermal stability, and optical properties of these two delafossite oxides have been studied at various stages of hydrothermal synthesis. It is believed that some mechanisms embedded in the synthesis of $CuAlO_2$ and $AgAlO_2$ is insightful for the preparation of other ternary delafossite oxides.

## 2. EXPERIMENTAL SECTION

All of the chemicals in these experiments were purchased from Sigma–Aldrich with analytical grade and used without further purification. In a typical hydrothermal synthesis process, certain amounts of reactants were dissolved/dispersed in deionized water, which were then transferred into the hastelloy autoclave (Model Parr 4576, Parr Instrument Company, USA; the usable temperature upper limit was 500 °C, and the pressure upper limit was 5000 psi) or the Teflon-lined autoclave (the usable temperature upper limit was 250 °C). The sealed autoclave was maintained at the selected temperature for reaction. After the reaction finished, the autoclave was naturally cooled to room temperature. Finally, the obtained precipitate was washed for several times in a centrifugal cleaning machine and was finally stored in absolute alcohol solution for further use.

Crystal phases of the powders were characterized by using a Panalytical X'pert Pro diffractometer (X-ray diffraction (XRD), Cu K$\alpha$ radiation) at room temperature. The microstructure and determine the composition of the as-synthesized crystals were observed using a field-emission scanning electron microscopy (FESEM) system (FEI-Nova NanoSEM 450) coupled with energy-dispersive X-ray spectroscopy (EDX). The thermal stability of crystals were investigated using a differential scanning calorimetry–thermogravimetric analysis (DSC-TG) device (Diamond TG/DTA, Perkin–Elmer Instruments), these samples were heated in air from room temperature to 1000 °C at a heating rate of 10 °C $min^{-1}$. The ultraviolet–visible–near infrared (UV-vis-NIR) spectroscopy of films was recorded on a Perkin–Elmer UV/vis spectrophotometer (UV-vis, Model Lambda 950) in the wavelength range of 300–800 nm. X-ray photoelectron spectroscopy (XPS) measurements were performed with Physical Electronics surface analysis equipment (Model PHI 5600), and the C (1s) line (at 285.0 eV) corresponding to the surface adventitious carbon (C–C line bond) has been used as the reference binding energy.

## 3. RESULTS AND DISCUSSION

**3.1. Synthesis of $CuAlO_2$ Crystals from CuCl and $NaAlO_2$.** $CuAlO_2$ crystals were prepared via a modified hydrothermal method from the literature.[3] At first, 10–25 mmol CuCl, 10 mmol $NaAlO_2$, and 0–0.6 g of NaOH were dissolved in 50 mL deionized water at room temperature. After reaching a homogeneous state, the solution was loaded into a 250 mL hastelloy autoclave (Parr Instrument Company, USA), which was sealed and maintained at 300–400 °C for 4 h. After the autoclave cooled to room temperature, the obtained blue-gray precipitate was washed with diluted hydrochloric acid solution (1 mol/L), diluted ammonia solution (1 mol/L), deionized water and absolute alcohol in sequence for several times, and then stored in absolute alcohol solution. Different reaction parameters, such as the molar ratios of the reactants (Cu/Al = 1:1, 1.5:1, 2:1, and 2.5:1), the mineralizer quantity (NaOH, 0, 0.2, and 0.6 g) and the synthesis temperature (300, 320, 360, and 400 °C) have been examined to find out the optimal conditions, as summarized in Table 1.

**Table 1. Details of the Reactions Conditions Employed To Synthesize $CuAlO_2$ Crystals from CuCl and $NaAlO_2$**

| Cu/Al ratio | temperature (°C) | NaOH (g) | phase composition |
|---|---|---|---|
| 1.0:1 | 400 | 0 | $CuAlO_2$,[b] AlOOH[a] |
| 1.5:1 | 400 | 0 | $CuAlO_2$,[a] AlOOH[b] |
| 2.0:1 | 400 | 0 | $CuAlO_2$,[a] AlOOH[b] |
| 2.5:1 | 400 | 0 | 3R-$CuAlO_2$, 2H-$CuAlO_2$ |
| 2.5:1 | 400 | 0.2 | 3R-$CuAlO_2$, 2H-$CuAlO_2$ |
| 2.5:1 | 400 | 0.6 | 3R-$CuAlO_2$ |
| 2.5:1 | 360 | 0.6 | 3R-$CuAlO_2$ |
| 2.5:1 | 320 | 0.6 | 3R-$CuAlO_2$, 2H-$CuAlO_2$ |
| 2.5:1 | 300 | 0.6 | $Cu_2O$, AlOOH |

[a]Majority phase. [b]Minor phase.

Figure 1 shows the XRD patterns of freshly obtained products from the starting materials with different Cu/Al ratios.

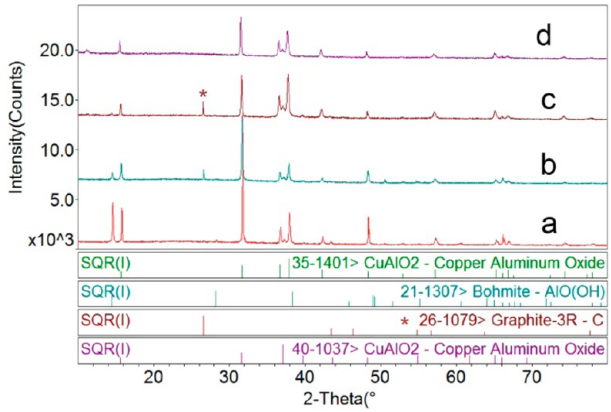


**Figure 1.** XRD patterns of freshly obtained products from reactants with different CuCl/$NaAlO_2$ ratios (1:1 (spectrum a), 1.5:1 (spectrum b), 2:1 (spectrum c), and 2.5:1 (spectrum d)).

The detailed synthetic conditions are as follows: 10–25 mmol CuCl and 10 mmol $NaAlO_2$ were dissolved/dispersed in 50 mL of deionized water and reacted at 400 °C for 4 h. When Cu/Al = 1:1, most of the diffraction peaks of products could be indexed as 3R-$CuAlO_2$ (rhombohedral, $R\bar{3}m$, JCPDS File Card No. 35-1401) and AlOOH (JCPDS File Card No. 21-1307) from Figure 1a, and very little 2H-$CuAlO_2$ (hexagonal, $P63/mmc$, JCPDS File Card No. 40–1037) also could be detected with a weak diffraction peak at 37.09°. Between these two crystal structure polytypes of $CuAlO_2$ (3R and 2H), the only difference is the stacking sequence of $ABO_2$ layers along the $c$-axis.[7] From Figure 1a, the diffraction peaks of AlOOH can be found with high intensity, suggesting the reaction products


dx.doi.org/10.1021/ic500090g | Inorg. Chem. 2014, 53, 4106–4116

contain a large fraction of AlOOH. In order to increase the yield of $CuAlO_2$, excessive amounts of CuCl were added as starting materials. Figures 1b–d show the XRD patterns of the products starting from reactants with the Cu/Al ratios of 1.5:1, 2:1, and 2.5:1, respectively. Comparing these XRD patterns in Figure 1, one could find that the diffraction peaks intensity of AlOOH gets weaker and weaker with increasing Cu/Al ratios from 1:1 to 2.5:1, indicating that the content of AlOOH in the products decreases gradually. At the Cu/Al ratio of 2.5:1, almost all of the aluminum source was exhausted, leading to pure $CuAlO_2$ product. This result raised a question: why should the quantity of CuCl be more excessive than the stoichiometric proportion of $CuAlO_2$ requires? It should be because some of the $Cu^+$ ions could be oxidized to $Cu^{2+}$ during the hydrothermal process, resulting in the formation of crystalline CuO, which, as demonstrated, has been washed off during the rinsing process. Furthermore, please note that the peaks labeled with an asterisk (*) in Figures 1b and 1c correspond to the graphite (JCPDS File Card No. 26-1079), which were derived from the graphite lubricants for sealing of the reaction vessel under high temperature.

In the previous report on the synthesis of $CuGaO_2$,[7] the NaOH/KOH concentration (pH value) in hydrothermal precursor has a strong impact on the morphology/crystal structure (3R or 2H) of the final product. In order to synthesize the single phase of 3R-$CuAlO_2$, a series of experiments have been carried out by adding different quantities of NaOH (0, 0.2, and 0.6 g) in the precursors containing 25 mmol CuCl and 10 mmol $NaAlO_2$. The hydrothermal reactions were undertaken at 400 °C for 4 h. By comparing the XRD patterns in Figure 2a, it is found that the crystalline $CuAlO_2$ could be obtained at any addition amounts of NaOH. In detail, two structural polytypes (3R and 2H) of $CuAlO_2$ have been formed without any NaOH addition. As the amount of NaOH increases, the diffraction peaks at 37.09°, which are due to

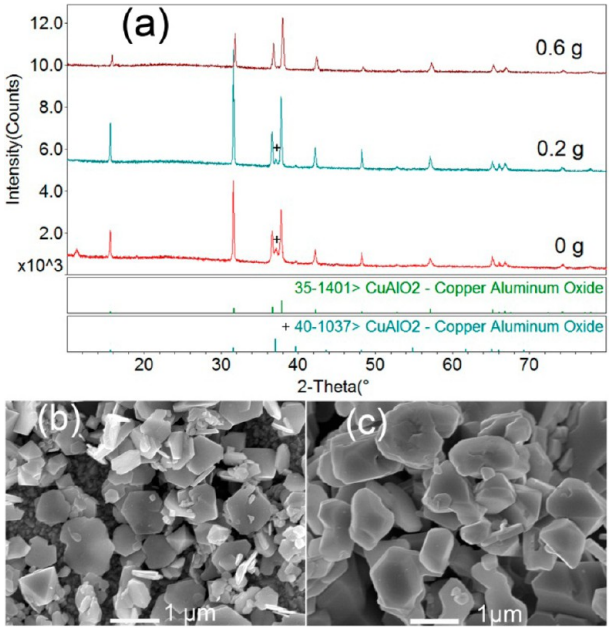


**Figure 2.** (a) XRD patterns of freshly obtained $CuAlO_2$ products from precursors with different NaOH quantities. Also shown are SEM images of freshly obtained $CuAlO_2$ products from precursors with different NaOH quantities: (b) 0 g and (c) 0.6 g.

the 2H-$CuAlO_2$ crystal phase (denoted by plus signs, "+") get weaker, indicating that the content of 2H-$CuAlO_2$ in the reaction products decreases gradually. At the NaOH quantity of 0.6 g, almost pure crystal phase of 3R-$CuAlO_2$ crystals could be obtained. SEM images in Figures 2b and 2c reflect that the addition of more NaOH mineralizer will promote Oswald ripening and result in bigger $CuAlO_2$ crystals with more uniform crystal phase and particle morphology.

To clarify the effect of hydrothermal temperature, a series of experiments have been carried out at different temperatures (300, 320, 360, and 400 °C) for preparing $CuAlO_2$ crystals. Twenty-five millimoles (25 mmol) of CuCl, 10 mmol of $NaAlO_2$, 0.6 g of NaOH dissolved in 50 mL deionized water were kept the same, and the reaction time was set unchanged at 4 h. From Figure 3a, when the reaction temperature decreases

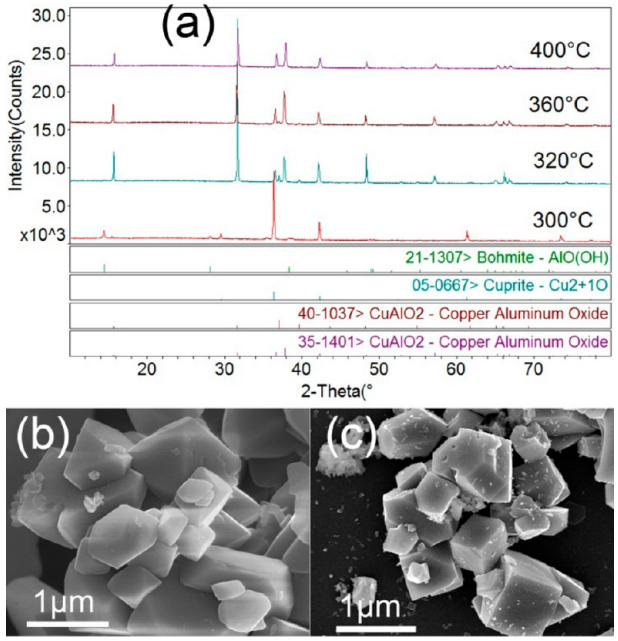


**Figure 3.** (a) XRD patterns of products freshly obtained from the hydrothermal synthesis of $CuAlO_2$ crystals from CuCl and $NaAlO_2$ at different reaction temperatures (300–400 °C). Also shown are SEM images of products freshly obtained from hydrothermal synthesis of $CuAlO_2$ crystals from CuCl and $NaAlO_2$ at different reaction temperatures ((b) 400 °C and (c) 320 °C).

from 400 °C to 320 °C, it can be identified from the XRD patterns that the reaction products remained almost unchanged as $CuAlO_2$ crystals. However, when further decreasing the reaction temperature to 300 °C, no $CuAlO_2$ is observed but the mixture of $Cu_2O$ (JCPDS File Card No. 05-0667) and AlOOH can be identified from the reaction products. It seems that 320 °C is a critical temperature for the phase formation of $CuAlO_2$. In addition, Figure 3b shows that both hexagonal and rhombohedral morphologies of $CuAlO_2$ crystals appear at the reaction temperature of 400 °C, and the sizes of these crystals are ~1 $\mu$m. For $CuAlO_2$ crystals synthesized at 320 °C, the average size is also ~1 $\mu$m, but the morphology of $CuAlO_2$ crystals slightly change to be more similar to rhombohedral crystals appearing in the product (see Figure 3c). These results are consistent with the XRD patterns shown in Figure 3a, indicating that more 2H-$CuAlO_2$ crystals (higher intensity of $2\theta$ at 37.09°) are included in the products, which are obtained at relatively lower reaction temperatures.


dx.doi.org/10.1021/ic500090g | Inorg. Chem. 2014, 53, 4106–4116

In this section, we have explored a series of parameters for the hydrothermal synthesis of $CuAlO_2$ crystals. In comparison to the previous studies,[3,34] in which the $CuAlO_2$ crystals were prepared by a 400 °C hydrothermal method, our facile synthetic conditions show a significant reduction on the synthesis temperature to 320 °C. However, it does not seem to be consistent with a previous reported in the literature.[3]

**3.2. Synthesis of $CuAlO_2$ Crystals from $Cu_2O$ and $Al_2O_3$ Nanoparticles.** The synthesis of nanometer-size $CuAlO_2$ is important for many photoelectrochemical applications, where a huge interface is required for efficient charge separation.[12−14]

As described in section 3.1, we have systematically studied the synthesis parameters effecting on the $CuAlO_2$ crystal formation starting from CuCl and $NaAlO_2$. Even when the hydrothermal synthesis temperature decreased to as low as 320 °C, it is hard to get small $CuAlO_2$ nanoparticles. In this section, we present the synthesis results of $CuAlO_2$ starting from nanosized $Cu_2O$ (~20 nm) and $Al_2O_3$ (~10 nm) instead of CuCl and $NaAlO_2$. Two to five millimoles (2−5 mmol) of $Cu_2O$ and 2−5 mmol of $Al_2O_3$ nanoparticles dispersed in 30−50 mL of deionized water were used as the starting materials. Different reaction parameters, such as the hydrothermal temperature (320, 340, 360, and 400 °C), the reaction time (1, 4, 8, and 12 h), and the filling ratios of the autoclave (30, 35, 40, and 50 mL of deionized water in a 250-mL autoclave) have been examined, as summarized in Table 2.

**Table 2. Details of the Reactions Conditions Employed To Synthesize $CuAlO_2$ Crystals from $Cu_2O$ and $Al_2O_3$ Nanoparticles**

| temperature (°C) | time (h) | pressure (psi) | phase composition |
|---|---|---|---|
| 400 | 4 | ~2800 (50 mL) | 3R-$CuAlO_2$ |
| 360 | 4 | ~2400 (50 mL) | $CuAlO_2$,[a] AlOOH[b] |
| 340 | 4 | ~2050 (50 mL) | $CuAlO_2$,[b] AlOOH[a] |
| 320 | 4 | ~1600 (50 mL) | $Cu_2O$, AlOOH |
| 340 | 1 | ~2050 (50 mL) | $CuAlO_2$,[a] AlOOH[b] |
| 340 | 4 | ~2050 (50 mL) | $CuAlO_2$,[a] AlOOH[b] |
| 340 | 8 | ~2050 (50 mL) | $CuAlO_2$, AlOOH |
| 340 | 12 | ~2050 (50 mL) | 3R-$CuAlO_2$ |
| 400 | 4 | ~1250 (30 mL) | 3R-$CuAlO_2$ |
| 400 | 4 | ~1600 (35 mL) | 3R-$CuAlO_2$ |
| 400 | 4 | ~1900 (40 mL) | 3R-$CuAlO_2$ |
| 400 | 4 | ~2800 (50 mL) | $CuAlO_2$, AlOOH |

[a]Majority phase. [b]Minor phase.

Figure 4 shows the XRD patterns and SEM images of the hydrothermal products obtained at different temperatures (300, 320, 360, and 400 °C). Two millimoles (2 mmol) of $Cu_2O$ and 2 mmol of $Al_2O_3$ dissolved in 50 mL of deionized water were used as the precursors and the reaction time was kept at 4 h for all of these reactions. From Figure 4a, the phase transition reaction from $Cu_2O$ and $Al_2O_3$ to $CuAlO_2$ did not occur at 320 °C, since there are only diffraction peaks owing to $Cu_2O$ and AlOOH could be detected in the XRD pattern. However, as the reaction temperature increases from 340 °C to 400 °C, the intensity of the diffraction peaks attributable to AlOOH gradually decreases and that of diffraction peaks corresponding to $CuAlO_2$ evidently increases. This result indicates that, at the elevated temperature, more and more AlOOH and $Cu_2O$ were consumed, leading to the formation of new $CuAlO_2$ crystals. When the reaction was carried out at 400 °C, the typical hexagonal morphology of $CuAlO_2$ crystals ~1−2 μm in size

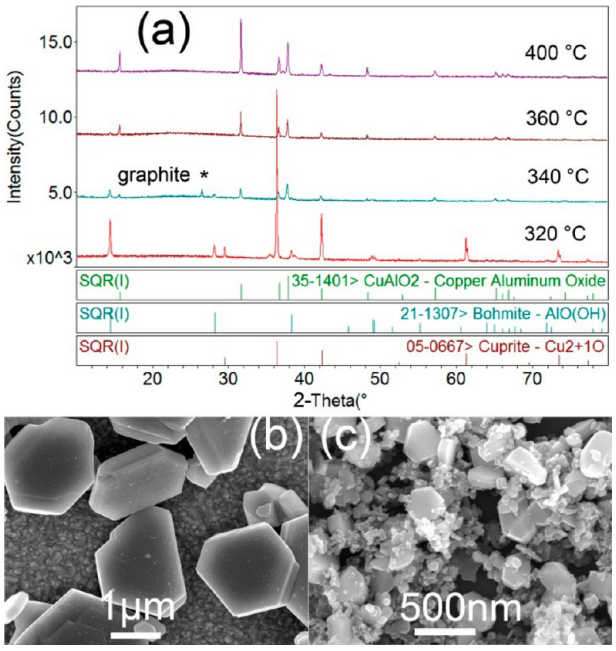


**Figure 4.** (a) XRD patterns of products freshly obtained from the hydrothermal synthesis of $CuAlO_2$ crystals from $Cu_2O$ and $Al_2O_3$ at different reaction temperatures (320−400 °C). Also shown are SEM images of freshly obtained products from the hydrothermal synthesis of $CuAlO_2$ crystals from $Cu_2O$ and $Al_2O_3$ at different reaction temperatures ((b) 400 °C and (c) 340 °C).

could be obtained (see Figure 4b). For the reaction product obtained at 340 °C, the hexagonal $CuAlO_2$ crystals were much smaller, ~300−400 nm in size. The much smaller nanoparticles (those <100 nm in size) should be the residual AlOOH (see Figure 4c). It seems to be difficult to obtain the nanosized $CuAlO_2$ crystals by simply adjusting the reaction temperature.

Figure 5 shows the XRD patterns and SEM images of the products obtained at different reaction times (such as 1, 4, 8, and 12 h). Five millimoles (5 mmol) of $Cu_2O$ and 5 mmol of $Al_2O_3$ nanoparticles dispersed in 50 mL of deionized water were used as the precursors, and all of the hydrothermal temperatures were set at 340 °C. When the reaction was maintained for 1 h, the main crystal phase of the product could be identified to be AlOOH, and a small amount of $CuAlO_2$ also appeared in it (Figure 5a). This result indicates that some of the $Al_2O_3$ and $Cu_2O$ started to convert to $CuAlO_2$ after 1 h of hydrothermal reaction. In addition, most of the crystals <150 nm in size could be identified as AlOOH (see Figure 5b), which was due to the high intensity of its diffraction peaks, suggesting the fast $Al_2O_3$ to AlOOH conversion in the first hour of hydrothermal reaction. With further extending the reaction time from 1 to 12 h, the intensity of the AlOOH diffraction peaks decreased gradually, suggesting that more AlOOH and $Cu_2O$ were exhausted and converted to $CuAlO_2$ crystals (Figure 5a). After the reaction was maintained for 12 h, almost-pure $CuAlO_2$ particles 100−300 nm in size were finally obtained (see Figures 5a and 5c), the size of which is almost the smallest that we have ever achieved.

In order to understand the effect of hydrothermal pressure on the crystal formation process of $CuAlO_2$ crystals, a series of experiments have been carried out with different filling ratios of the autoclave. Briefly, 5 mmol of $Cu_2O$ and 5 mmol of $Al_2O_3$ were dispersed in 30−50 mL of deionized water and kept at 400 °C for 4 h. The hydrothermal pressure was found to be


dx.doi.org/10.1021/ic500090g | Inorg. Chem. 2014, 53, 4106−4116

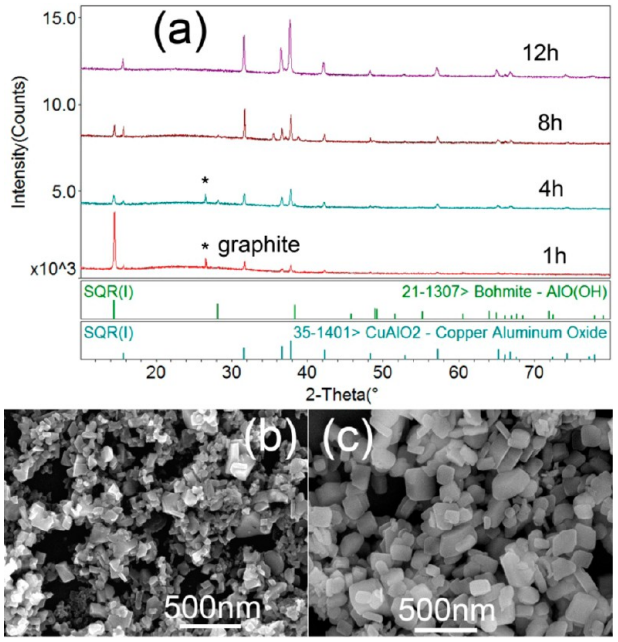


**Figure 5.** (a) XRD patterns of reaction products freshly obtained from the hydrothermal synthesis of $CuAlO_2$ crystals from $Cu_2O$ and $Al_2O_3$ with different reaction time at 340 °C (1−12 h). Also shown are SEM images of reaction products freshly obtained from the hydrothermal synthesis of $CuAlO_2$ crystals from $Cu_2O$ and $Al_2O_3$ with different reaction times at 340 °C ((b) 1 h and (c) 12 h).

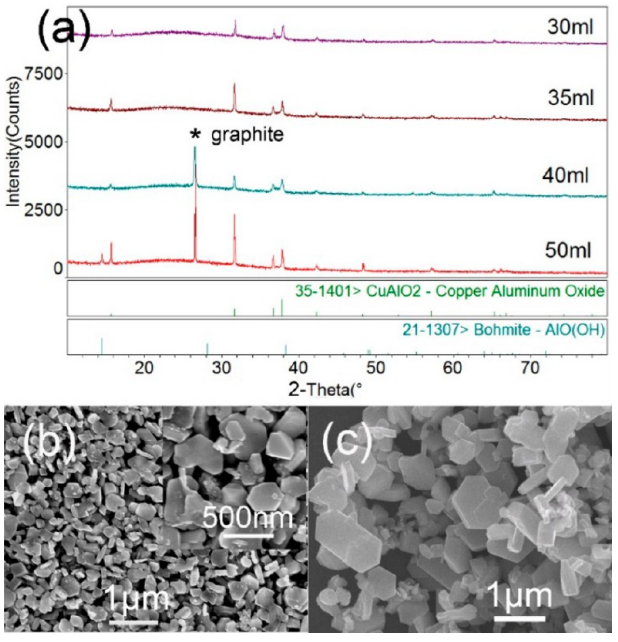


**Figure 6.** (a) XRD patterns of reaction products freshly obtained from the hydrothermal synthesis of $CuAlO_2$ crystals from $Cu_2O$ and $Al_2O_3$ with different volumes of deionized water (30−50 mL). Also shown are SEM images of reaction products freshly obtained from the hydrothermal synthesis of $CuAlO_2$ crystals from $Cu_2O$ and $Al_2O_3$ with different volumes of deionized water ((b) 30 mL and (d) 50 mL).

determined by the filling ratios of the autoclave. For example, the hydrothermal pressures read from the pressure meter of the autoclave are ∼1250, 1600, 1900, and 2800 psi, corresponding to 30, 35, 40, and 50 mL of deionized water in a 250-mL autoclave, respectively. Figure 6a shows that, from the XRD patterns, the intensity of peaks of $CuAlO_2$ is stronger when the water volume (hydrothermal pressure) is higher. The result is consistent with the SEM observations: at a water volume of 30 mL, the $CuAlO_2$ crystals are ∼300−500 nm (Figure 6b), while at a water volume of 50 mL, the $CuAlO_2$ crystals are ∼1 $\mu$m in size. Moreover, if comparing the $CuAlO_2$ particles in Figures 4b and 6c, it is obvious that the latter one is even smaller in size (∼1 $\mu$m vs ∼1.5 $\mu$m). Note that these two products were both synthesized at 400 °C for 4 h and the filling ratio was also 50 mL/250 mL. The only difference was the concentrations of reactants: the former concentration was 2 mmol and the latter concentration was 5 mmol. This comparison reflects that higher concentrations of reactants may lead to a higher concentration of crystal seeds, rather than no increases in the crystal growth rate, and, therefore, smaller $CuAlO_2$ particulate product.

As mentioned above, we have described a hydrothermal method for producing submicrometer-sized (<500 nm) $CuAlO_2$ crystals, using $Cu_2O$ and $Al_2O_3$ nanoparticles as starting materials. The wide synthetic conditions of temperature−pressure range from 400 °C−1250 psi to 340 °C−2050 psi. The changes of reaction reactants (replacing the starting materials of CuCl and $NaAlO_2$ by $Cu_2O$ and $Al_2O_3$) have an obvious effect on the morphologies of the $CuAlO_2$ crystals (from >1 $\mu$m to <300 nm), but all attempts to synthesize $CuAlO_2$ nanocrystals have failed. It seems very difficult to obtain nanosized $CuAlO_2$ crystals based on the present experimental conditions, which may be due to the self-defect of hydrothermal synthesis method, especially in the conditions of supercritical temperature range and extremely high pressure.

To analyze the chemical compositions of $CuAlO_2$ crystals, SEM-EDS mapping scan was employed to characterize the powders deposited on a silicon wafer substrate. The results are shown in Figure 7. It can be observed that all of the elemental

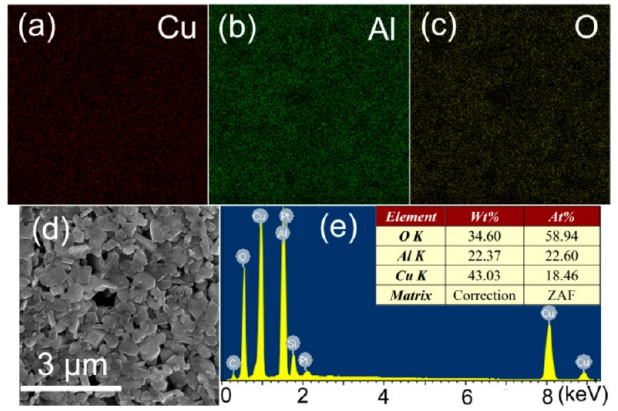


**Figure 7.** (a−c) EDS elemental mapping, (d) SEM image, and (e) elemental analysis report of the $CuAlO_2$.

copper, aluminum, and oxygen are homogeneously distributed, the elemental percentages of Cu (18.46 at. %), Al (22.60 at. %), and O (58.94 at. %) are consistent with the concentrations of their source materials in the hydrothermal precursor and match well with the stoichiometric proportion of $CuAlO_2$. Furthermore, the elemental chemical states of the $CuAlO_2$ crystals have been investigated by XPS. The corresponding results are shown in Figure 8; it can be seen that the peaks located at ∼932.5 and 952.4 eV (Figure 8a) correspond to the binding energies of Cu $2p_{3/2}$ and Cu $2p_{1/2}$, which confirm the monovalent state of copper ($Cu^+$).[15,35] The peak close to 74.2 eV (Figure 8b) is


dx.doi.org/10.1021/ic500090g | Inorg. Chem. 2014, 53, 4106−4116

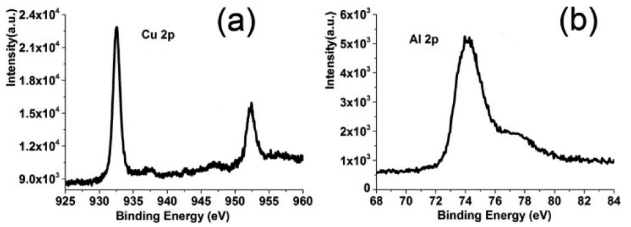


**Figure 8.** Typical XPS spectra of $CuAlO_2$: (a) Cu 2p and (b) Al 2p.

corresponding to the binding energies of Al 2p, which confirm the trivalent state of aluminum ($Al^{3+}$).[36]

**3.3. Hydrothermal Synthesis of $AgAlO_2$ Crystals.** In this section, $AgAlO_2$ crystals were prepared via a similar hydrothermal method modified from our previously reports on the synthesis of $CuCrO_2$.[15−17] In a typical synthesis, 15 mmol $Al(NO_3)_3{\cdot}9H_2O$ and 15 mmol $AgNO_3$ were dissolved in 70 mL of deionized water at room temperature; 2.40 g NaOH was added to the above solution and stirred for 10 min. After reaching a homogeneous state, the solution was loaded into a 100 mL Teflon-lined autoclave, which was sealed and maintained at 170- 210 °C for 60 h. Then, the obtained white-gray precipitate was washed with diluted nitric acid (1 mol/L), diluted ammonia (1 mol/L), deionized water and absolute alcohol in sequence for several times, and then stored in absolute alcohol solution. Similar to the synthesis procedure of $CuAlO_2$ crystals, different reaction parameters—such as the pH values of hydrothermal precursor (pH 5.40, 7.10, 8.50, 10.70, and 12.50) and the synthesis temperature (170, 190, and 210 °C)—have been examined to determine the optimal conditions; the details are summarized in Table 3.

**Table 3. Details of the Reactions Conditions Employed To Synthesize $AgAlO_2$ Crystals**

| temperature (°C) | pH value | phase composition |
|---|---|---|
| 210 | 5.40 | AlOOH |
| 210 | 7.10 | $AgAlO_2$, AlOOH |
| 210 | 8.50 | 3R-$AgAlO_2$ |
| 210 | 10.70 | 3R-$AgAlO_2$ |
| 210 | 12.50 | 3R-$AgAlO_2$ |
| 190 | 8.50 | 3R-$AgAlO_2$ |
| 170 | 8.50 | $AgO_2$, AlOOH |

As previously mentioned, the pH value of the precursor has a strong impact on the final reaction product during the hydrothermal synthesis. In order to analyze the formation process of $AgAlO_2$ crystals associated with pH values, a series of experiments have been carried out with different pH values of the precursors (such as pH 5.40, 7.10, 8.50, 10.70, and 12.50). In detail, 15 mmol of $Al(NO_3)_3{\cdot}9H_2O$, 15 mmol of $AgNO_3$, and 2.40 g of NaOH were dissolved in 70 mL of deionized water, and the pH value was adjusted by adding either dilute nitric acid solution (1 mol/L) or dilute sodium hydroxide solution (1 mol/L) dropwise, and, finally, the sealed autoclave was maintained at 210 °C for 60 h.

Figure 9 shows the XRD patterns and SEM images of the as-prepared products. At the pH value of 5.40, all observed diffraction peaks could be indexed to be AlOOH (see Figure 9a); there is no diffraction peak for elemental silver, mainly because the silver was maintained as stable ions in acid solution. The XRD result is very consistent with the SEM image, as shown in Figure 9b. The rodlike AlOOH nanocrystals with a uniform size of 300 nm × 50 nm are observed in the reaction products, and the morphology of AlOOH is clearly quite different from the other crystals, as shown in Figure 9. As the pH value increases to 7.10, the XRD pattern (Figure 9a) indicates that both AlOOH and $AgAlO_2$ are present in the product, and the crystal size is ∼50−200 nm (see Figure 9c). When the pH value was further adjusted to >7.10 (such as 8.50, 10.70, and 12.50), the XRD peaks of these products could be similarly assigned to pure $AgAlO_2$. These XRD results are in good agreement with the SEM results shown in Figures 9d−f. The $AgAlO_2$ crystals have similar hexagonal laminar morphologies, and as the pH values of the precursors increase, the crystal size increases accordingly, from ∼200 nm to ∼1 μm. The results demonstrate that the alkaline precursor conditions favor $AgAlO_2$ crystal growth.[7] Furthermore, in order to clarify the effect of hydrothermal temperature, several hydrothermal reactions have been carried out at 210, 190, and 170 °C, respectively, while the pH values were set unchanged at 8.50 for these reactions. When the reaction temperature decreases from 210 °C to 190 °C, the XRD and SEM results indicate that pure $AgAlO_2$ crystals with a smaller size (∼100−300 nm) could be obtained (Figure 10). When the reaction temperature is reduced further, to 170 °C, the reaction products could be identified, from the XRD patterns, as a mixture of AlOOH (JCPDS File Card No. 21-1307) and $Ag_2O$ (JCPDS File Card No. 65-3289) (Figure 10a), indicating that the reaction temperature of 170 °C is too low to generate $AgAlO_2$ crystals.

Figure 11 shows the SEM-EDS mapping results of $AgAlO_2$ crystals. It could be found that all of the elemental silver, aluminum, and oxygen are homogeneously distributed; the elemental percentages of Ag (21.19 at. %), Al (18.87 at. %), and O (59.93 at. %) are almost consistent with the concentrations of their source materials in the hydrothermal precursor. In addition, the XPS results of $AgAlO_2$ crystals are presented in Figure 12. The peak located at 73.8 eV (Figure 12a) corresponds to the binding energies of Al 2p, which confirms the trivalent state of aluminum ($Al^{3+}$).[36] The peaks located at 368.5 and 374.5 eV (Figure 12b) correspond to the binding energies of Ag $3d_{5/2}$ and Ag $3d_{3/2}$, which confirm the monovalent state of silver ($Ag^+$).[33]

As mentioned above, we have described a low-temperature hydrothermal method for preparing submicrometer-sized (<500 nm) $AgAlO_2$ crystals. In comparison to recently reported supercritical hydrothermal (>400 °C) synthesis of $AgCrO_2$,[33] the reaction parameters in this work are much more gentle and energy-saving. Although, after roughly optimizing the pH value and reaction temperature, the smallest size of as-synthesized $AgAlO_2$ crystals is even bigger than 100 nm, it still has much room for further optimizations on the parameters such as reaction time, concentrations of starting reactants, additives, etc.

**3.4. Thermal Stability of $CuAlO_2$ and $AgAlO_2$ Crystals.** From the thermogravimetric (TG) curves shown in Figures 13a and 13c, the initial weight loss may be due to the evaporation of chemically combined water of crystallization and the variation of oxygen vacancy in the samples. Figure 13a shows that the mass of $CuAlO_2$ increases sharply above 800 °C in air, which should be due to the oxidation of $CuAlO_2$ (the monovalent copper ($Cu^+$) was oxidized into divalent copper ($Cu^{2+}$)).[15,37] The XRD patterns (Figure 13b) of the samples sintered at different temperatures support this point. For example, all of the diffraction peaks could be indexed as pure $CuAlO_2$ (JCPDS File Card No. 35-1401) after the sample was sintered at 600 °C


dx.doi.org/10.1021/ic500090g | Inorg. Chem. 2014, 53, 4106−4116

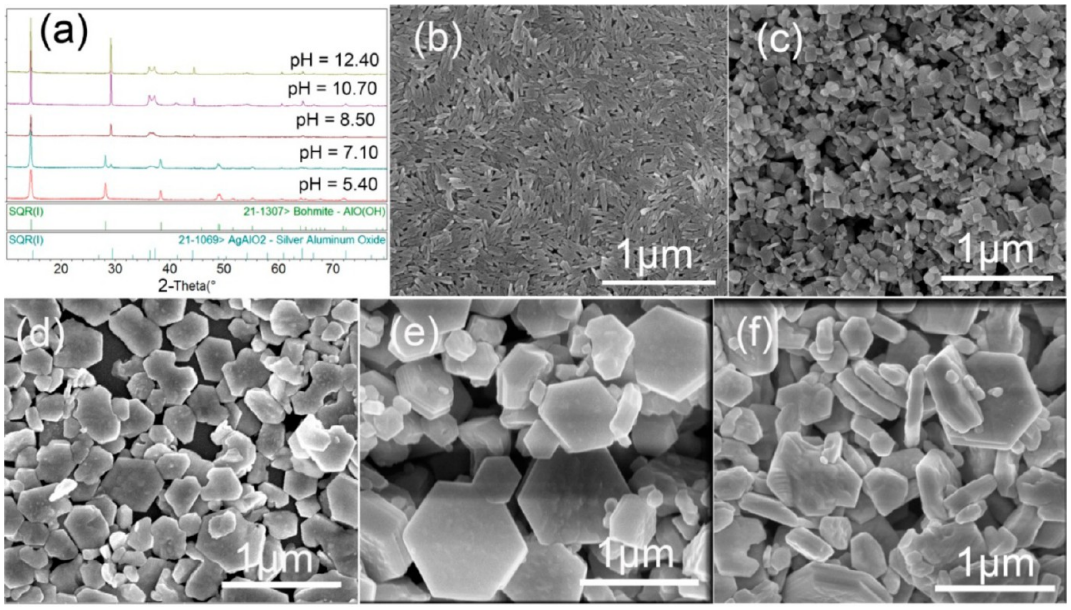


**Figure 9.** (a) XRD patterns of freshly obtained reaction products with different pH values of precursors for $AgAlO_2$ preparation. Also shown are corresponding SEM images of freshly obtained reaction products with different pH values ((b) 5.40, (c) 7.10, (d) 8.50, (e) 10.70, and (f) 12.50) of precursors for $AgAlO_2$ preparation at 210 °C.

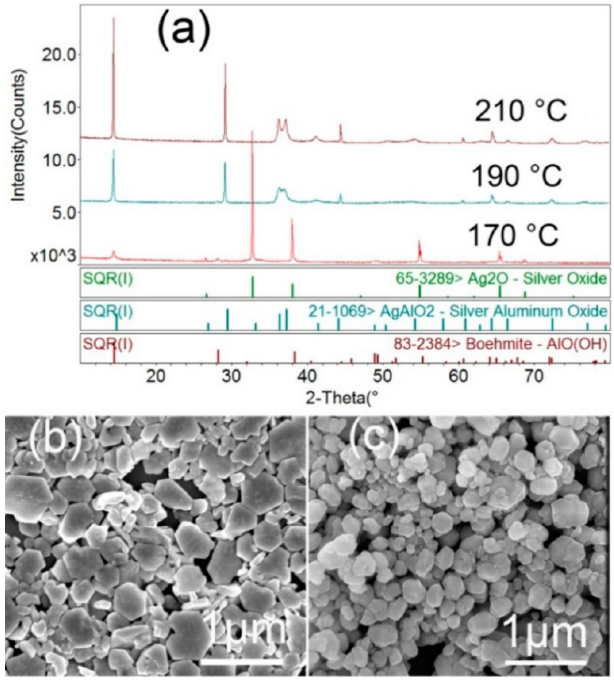


**Figure 10.** (a) XRD patterns of fresh reaction products obtained at different reaction temperatures (170−210 °C). Also shown are SEM images of fresh reaction products obtained at different reaction temperatures ((b) 210 °C and (c) 190 °C).

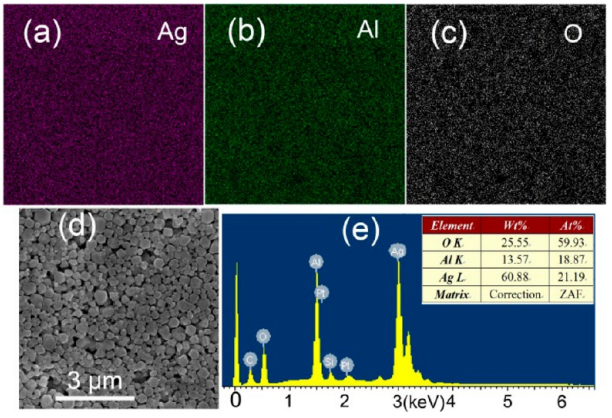


**Figure 11.** (a−c) EDS elemental mapping, (d) SEM image, and (e) elemental analysis report of the $AgAlO_2$.

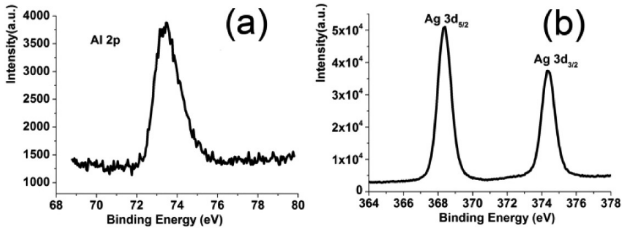


**Figure 12.** Typical XPS spectra of $AgAlO_2$: (a) Al 2p and (b) Ag 3d.

in air for 1 h, and no impurity phase could be detected. After the sample was sintered at 800 °C, besides $CuAlO_2$, the diffraction peaks that can be attributed to new crystal phases of CuO (JCPDS File Card No. 41-0254) and $CuAl_2O_4$ (JCPDS File Card No. 33-0448) could be detected, which is suggested to be derived from partial oxidization of $CuAlO_2$ crystals. Moreover, only CuO and $CuAl_2O_4$ phases could be found after the $CuAlO_2$ sample was sintered at 1000 °C, which suggests that the oxidization reaction of delafossite $CuAlO_2$ has been almost completed. Based on the consistent XRD and TG results, it is suggested that the following chemical reaction should be involved during the high-temperature (>800 °C) sintering:

$$4CuAlO_2 + O_2 = 2CuAl_2O_4 + 2CuO \quad (1)$$

According to recently published papers on the synthesis of $CuAlO_2$ by solid-state reactions,[12,38] $CuAlO_2$ could be synthesized at relatively low temperatures of 750−800 °C


dx.doi.org/10.1021/ic500090g | Inorg. Chem. 2014, 53, 4106−4116

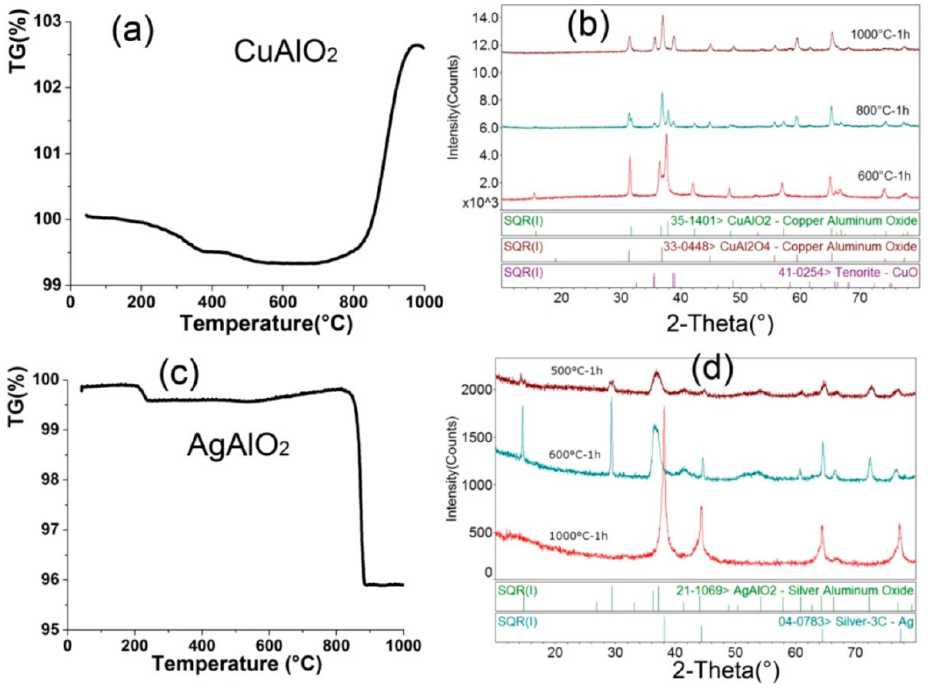


**Figure 13.** Thermogravimetric (TG) curves of (a) $CuAlO_2$ and (c) $AgAlO_2$ at a heating rate of 10 °C $min^{-1}$ in air. Also shown are the corresponding XRD patterns for (b) $CuAlO_2$ and (d) $AgAlO_2$ powder after sintering in air at different temperatures.

under $N_2$ or a high vacuum atmosphere, but if sintered in air, $CuAlO_2$ crystal phase could only be present at temperatures higher than 1100 °C. The results also indicate that the thermal stability of $CuAlO_2$ is closely related to the partial pressure of oxygen during sintering. It is interesting that the mass of $AgAlO_2$ decreases sharply above 800 °C (Figure 13c), implying a totally different decomposition mechanism from that of $CuAlO_2$ during high-temperature sintering.[6] Figure 13d shows the XRD patterns of $AgAlO_2$ samples sintered at different temperatures. For the sample that was sintered at 500 or 600 °C in air for 1 h, they have similar patterns, which could be identified as pure $AgAlO_2$ crystal phase. However, after the sample was sintered at 1000 °C in air for 1 h, diffraction peaks that could be attributed to the newly generated elemental silver (JCPDS File Card No. 04-0783) could be detected (Figure 13d), suggesting that the $AgAlO_2$ crystal decomposed to Ag and $Al_2O_3$ at 1000 °C. This phenomenon is consistent with TG analysis. It is suggested that the following chemical reaction should be involved during high-temperature (>800 °C) sintering:

$$4AgAlO_2 = 2Al_2O_3 + 4Ag + O_2 \quad (2)$$

Besides, it should be noted that a fast temperature ramping process (10 °C/min) was applied during TG analysis; therefore, it may lead to underestimation of the mass changes in comparison to the theoretical values calculated on the basis of the chemical reactions.[39] For example, according to eq 1, the full oxidization of $CuAlO_2$ should lead to a theoretical mass increase of 6.53%, but the tested mass increase was only 3.24% (Figure 13a). In a similar case, the monitored value of weight loss for $AgAlO_2$ after high-temperature sintering was only 3.97% (Figure 13c), which is also relatively lower than the calculated value (4.79%) obtained from the decomposition reaction of eq 2.

**3.5. Optical Properties.** In order to study the optical properties of $CuAlO_2$ and $AgAlO_2$ crystals, uniform films were prepared on the glass slides through spray deposition method. After the films were heated in air at 300 °C for 1 h, the UV-vis spectroscopy was employed to examine the optical transmittance of these films. The optical band gap was estimated by the following equation:[40]

$$(\alpha\hbar\nu)^{1/n} = A(\hbar\nu - E_g) \quad (3)$$

where $\alpha$ is the absorption coefficient, $\hbar$ is Planck's constant, $\nu$ is the frequency of light, $A$ is a constant, and $E_g$ is the band gap. Moreover, the exponent $n$ depends on the type of transition: for direct-allowed transition, $n = 1/2$; for indirect-allowed transition, $n = 2$; for direct-forbidden transition, $n = 3/2$; and for direct-forbidden transition, $n = 3$.[40] Figure 14 shows the optical transmittance spectra within the wavelength range of 300−800 nm and the calculated bandgaps of $CuAlO_2$ and $AgAlO_2$ films. From Figure 14a, the transmittance for the blue-gray $CuAlO_2$ film (0.5 $\mu$m) is ~60%−85% in the visible range. The calculated values of the direct band gaps for $CuAlO_2$ is 3.48 eV (Figure 14a), which is consistent with the earlier report.[3] For the $AgAlO_2$ crystals, the transmittance of the white-gray $AgAlO_2$ film (~0.6 $\mu$m) is even better than that of the $CuAlO_2$ film, which is above 80% in the entire visible range (Figure 14b). The calculated values of direct band gaps for $AgAlO_2$ is 3.89 eV (Figure 14b), which is close to the value reported earlier on the band gap (3.6 eV).[6] If one compares the band-gap values of $CuAlO_2$ and $AgAlO_2$, the larger optical band gap of $AgAlO_2$ is suggested to be due to a shift of the valence band states toward lower energy, associated with the replacement of Cu 3d states with Ag 4d states.[6]

**3.6. The Proposed Synthesis Mechanisms.** High-temperature solid-state reaction and hydrothermal reaction are the most common methods used for preparing the delafossite oxides ($CuAlO_2$ and $AgAlO_2$). Recently, several papers that were dedicated to understanding the synthesis mechanisms involved in the solid-state reactions have been published.[38,39] However, until now, there has been few


dx.doi.org/10.1021/ic500090g | Inorg. Chem. 2014, 53, 4106−4116

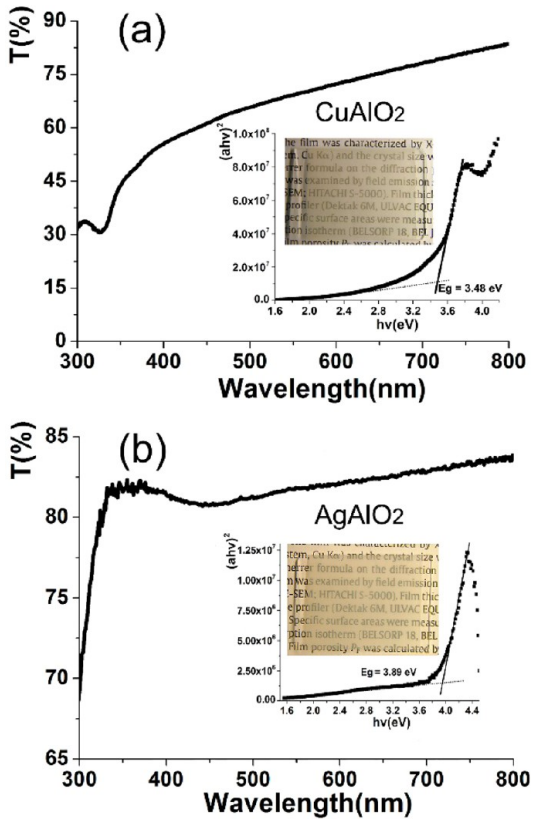


**Figure 14.** Optical transmittance of (a) $CuAlO_2$ and (b) $AgAlO_2$; the insets show the corresponding optical images and calculated direct bandgap.

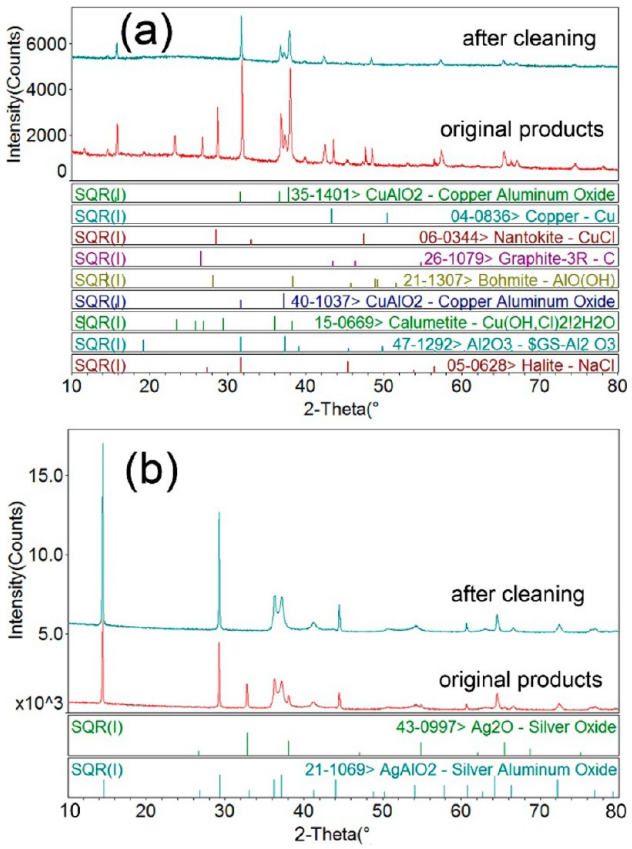


**Figure 15.** XRD patterns of reaction products for the preparation of (a) $CuAlO_2$ and (b) $AgAlO_2$.

literature that has focused on the hydrothermal synthesis mechanisms. In this work, first, we synthesized $CuAlO_2$ crystals from $NaAlO_2$, CuCl, and NaOH. From the XRD patterns in Figure 15a, it can be seen that CuCl, Cu, CuO, $CuAlO_2$, AlOOH, $Al_2O_3$, and NaCl were all detected in the origin reaction product. After washing with diluted hydrochloric acid, diluted ammonia, and absolute alcohol, only $CuAlO_2$, $Al_2O_3$ and AlOOH crystal phases could remain in the reaction product. Others were dissolved and washed off as ions. The synthetic process could be described by the following reaction equations:

$$CuCl(s) + H_2O(l) = Cu_2O(s) + HCl(aq) \quad (4a)$$

$$Cu_2O(s) = Cu(s) + CuO(s) \quad (4b)$$

$$NaAlO_2(aq) + HCl(aq) = HAlO_2(aq) + NaCl(aq) \quad (4c)$$

$$AlO_2^-(aq) + 4H^+(aq) = Al^{3+}(aq) + 2H_2O(l) \quad (4d)$$

$$Al^{3+}(aq) + 3OH^-(aq) = Al(OH)_3(s) \quad (4e)$$

$$Al(OH)_3(s) = AlOOH(s) + H_2O(l) = \frac{1}{2}Al_2O_3(s) + \frac{3}{2}H_2O(l) \quad (4f)$$

$$Cu_2O(s) + 2AlOOH(s) = 2CuAlO_2(s) + H_2O(l) \quad (4g)$$

When the starting materials were $Al_2O_3$ and $Cu_2O$, both $CuAlO_2$ and AlOOH were detected in the reaction product after the washing procedure. The reaction equations should be written as follows:

$$Al_2O_3(s) + 3H_2O(l) = 2Al(OH)_3(s) \quad (5a)$$

$$Al(OH)_3(s) = AlOOH(s) + H_2O(l) \quad (5b)$$

$$Cu_2O(s) + 2AlOOH(s) = 2CuAlO_2(s) + H_2O(l) \quad (5c)$$

From the above results and analysis, we can concluded that, under hydrothermal conditions, the chemical reactions for the synthesis of $CuAlO_2$ is a complicated process, rather than just a cation exchange reaction, CuCl + $NaAlO_2$ = NaCl + $CuAlO_2$, as described in a previous report.[3] The key step is to form $Cu_2O$ and AlOOH crystal seeds from $Cu_2O$, which leads to the subsequent formation and growth of $CuAlO_2$. This is almost the same reaction taking place during the high-temperature solid-state reaction.[4,41] However, it should be: because of the large hydrothermal pressure, the synthesis temperature can be dramatically reduced from above 1000 °C to 320 °C.

Besides, $AgAlO_2$ crystals were obtained from the hydrothermal reaction of two metal nitrates ($Al(NO_3)_3$ and $AgNO_3$) with sodium hydroxide (NaOH) as a mineralizer, at a hydrothermal temperature of 190−210 °C. From the XRD patterns in Figure 15b, it can be seen that the origin reaction product contains $Ag_2O$ and $AgAlO_2$, and we can get pure $AgAlO_2$ crystals after the washing procedure. Combined with the analysis of XRD patterns in Figure 10a, both AlOOH and $Ag_2O$ were observed in reaction product obtained at 170 °C, it can be concluded that the substitutional reactions and combination reaction should occur during the synthetic


dx.doi.org/10.1021/ic500090g | Inorg. Chem. 2014, 53, 4106−4116

process, which should be written as the following reaction equations:

$$AgNO_3(aq) + NaOH(aq) = AgOH(s) + NaNO_3(aq) \quad (6a)$$

$$2AgOH(s) = Ag_2O(s) + H_2O \quad (6b)$$

$$Al(NO_3)_3(s) + 3NaOH(s) = Al(OH)_3(s) + 3NaNO_3(aq) \quad (6c)$$

$$Al(OH)_3(s) = AlOOH(s) + H_2O(l) \quad (6d)$$

$$Ag_2O(s) + 2AlOOH(s) = 2AgAlO_2(s) + H_2O(l) \quad (6e)$$

## 4. CONCLUSIONS

In summary, we report the systematic results on the hydrothermal synthesis of wide-band-gap (>3.10 eV) delafossite oxides of $CuAlO_2$ and $AgAlO_2$ particles with high thermal stability (>800 °C) and high optical transparency (60−85%). The synthesis temperatures for $CuAlO_2$ and $AgAlO_2$ have been expanded to as low as 320 and 190 °C, respectively. During the synthesis process of $CuAlO_2$ crystals, in comparison to the hydrothermal synthesis conditions (such as synthesis temperature, pH value, reaction time, and pressure), the selection of starting reactants (CuCl + $NaAlO_2$ or $Cu_2O$ + $Al_2O_3$) has a significant effect on the crystal size and morphology of $CuAlO_2$. In particular, we have successful synthesized submicrometer-sized (100−300 nm) $CuAlO_2$ crystals through a single-step hydrothermal reaction from $Cu_2O$ and $Al_2O_3$ nanoparticles at 340 °C. For the hydrothermal synthesis of $AgAlO_2$ crystals, the pH value of precursor has a strong impact on crystal phase and morphology in final product. Just like $CuAlO_2$ crystals, the alkaline conditions of the precursor favored the formation of delafossite oxides with 3R crystals (3R-$AgAlO_2$). We have synthesized submicrometer-sized (300−500 nm) $AgAlO_2$ crystals through a simple one-step hydrothermal reaction at 190 °C from two metal nitrates ($Al(NO_3)_3$ and $AgNO_3$) with sodium hydroxide (NaOH) as a mineralizer. Furthermore, according to the analysis of reaction products generated during the hydrothermal process, we have proposed the synthesis mechanism for $CuAlO_2$ and $AgAlO_2$ crystals. The specific synthesis mechanism for these low-temperature hydrothermal methods is similar to that in the high-temperature solid-state reaction, namely, two Al-based delafossite oxides ($CuAlO_2$ and $AgAlO_2$) may be formed from the reaction between AlOOH and the corresponding metal oxide with monovalent ($Cu_2O$ and $Ag_2O$). This proposed synthesis mechanism could open a new route for the preparation of other delafossite oxides.

## AUTHOR INFORMATION


### Corresponding Author

*Tel.: 86 8779 3867. Fax: 86 8779 3867. E-mail: wnlochenwei@hust.edu.cn.


### Author Contributions

All authors have given approval to the final version of the manuscript.

### Notes

The authors declare no competing financial interest.

## ACKNOWLEDGMENTS


The authors would like to express sincere thanks for the financial support by the National Natural Science Foundation (No. 21103058), 973 Program of China (No. 2011CBA00703), and Basic Scientific Research Fund for Central Colleges (Nos. 2012YQ027 and 2013TS040). D. Xiong also thanks the financially support by the Fundamental Research Fund for the Central Universities (WUT: 2014-IV-091). We also thank Analytical and Testing Center of Huazhong University Science & Technology for the sample measurements.


## REFERENCES


(1) Kawazoe, H.; Yasukawa, M.; Hyodo, H.; Kurita, M.; Yanagi, H.; Hosono, H. *Nature* **1997**, *389*, 939−942.
(2) Shannon, R. D.; Rogers, D. B.; Prewitt, C. T. *Inorg. Chem.* **1971**, *10*, 713−718.
(3) Shanmin, G.; Yan, Z.; Pingping, G.; Nan, C.; Yi, X. *Nanotechnology* **2003**, *14*, 538.
(4) Ingram, B. J.; González, G. B.; Mason, T. O.; Shahriari, D. Y.; Barnabè, A.; Ko, D.; Poeppelmeier, K. R. *Chem. Mater.* **2004**, *16*, 5616−5622.
(5) Sheets, W. C.; Mugnier, E.; Barnabé, A.; Marks, T. J.; Poeppelmeier, K. R. *Chem. Mater.* **2006**, *18*, 7−20.
(6) Sheets, W. C.; Stampler, E. S.; Bertoni, M. I.; Sasaki, M.; Marks, T. J.; Mason, T. O.; Poeppelmeier, K. R. *Inorg. Chem.* **2008**, *47*, 2696−2705.
(7) Srinivasan, R.; Chavillon, B.; Doussier-Brochard, C.; Cario, L.; Paris, M.; Gautron, E.; Deniard, P.; Odobel, F.; Jobic, S. *J. Mater. Chem.* **2008**, *18*, 5647.
(8) Durá, O. J.; Boada, R.; Rivera-Calzada, A.; León, C.; Bauer, E.; de la Torre, M. A. L.; Chaboy, J. *Phys. Rev. B* **2011**, *83*, 045202.
(9) Lekse, J. W.; Underwood, M. K.; Lewis, J. P.; Matranga, C. *J. Phys. Chem. C* **2012**, *116*, 1865−1872.
(10) Kawazoe, H.; Yanagi, H.; Ueda, K.; Hosono, H. *MRS Bull.* **2000**, *25*, 28−36.
(11) Dong, H.; Li, Z.; Xu, X.; Ding, Z.; Wu, L.; Wang, X.; Fu, X. *Appl. Catal., B* **2009**, *89*, 551−556.
(12) Nattestad, A.; Zhang, X.; Bach, U.; Cheng, Y.-B. *J. Photonics Energy* **2011**, *1*, 011103-1−011103-9.
(13) Yu, M.; Natu, G.; Ji, Z.; Wu, Y. *J. Phys. Chem. Lett.* **2012**, *3*, 1074−1078.
(14) Renaud, A.; Chavillon, B.; Le Pleux, L.; Pellegrin, Y.; Blart, E.; Boujtita, M.; Pauporté, T.; Cario, L.; Jobic, S.; Odobel, F. *J. Mater. Chem.* **2012**, *22*, 14353.
(15) Xiong, D.; Xu, Z.; Zeng, X.; Zhang, W.; Chen, W.; Xu, X.; Wang, M.; Cheng, Y.-B. *J. Mater. Chem.* **2012**, *22*, 24760.
(16) Xiong, D.; Zhang, W.; Zeng, X.; Xu, Z.; Chen, W.; Cui, J.; Wang, M.; Sun, L.; Cheng, Y. B. *ChemSusChem* **2013**, *6*, 1432−1437.
(17) Xu, X.; Zhang, B.; Cui, J.; Xiong, D.; Shen, Y.; Chen, W.; Sun, L.; Cheng, Y.; Wang, M. *Nanoscale* **2013**, *5*, 7963−7969.
(18) Xu, Z.; Xiong, D.; Wang, H.; Zhang, W.; Zeng, X.; Ming, L.; Chen, W.; Xu, X.; Cui, J.; Wang, M.; Powar, S.; Bach, U.; Cheng, Y.-B. *J. Mater. Chem. A* **2014**, *2*, 2968−2976.
(19) Amrute, A. P.; Larrazábal, G. O.; Mondelli, C.; Pérez-Ramírez, J. *Angew. Chem., Int. Ed.* **2013**, *52*, 9772−9775.
(20) Veselovskyi, V. L.; Ischenko, E. V.; Gayday, S. V.; Byeda, A.; Tkach, V. V.; Lisnyak, V. V. *Curr. Catal.* **2013**, *2*, 7−12.
(21) Thu, T. V.; Thanh, P. D.; Suekuni, K.; Hai, N. H.; Mott, D.; Koyano, M.; Maenosono, S. *Mater. Res. Bull.* **2011**, *46*, 1819−1827.
(22) Chen, H.-Y.; Chang, K.-P. *ECS J. Solid State Sci. Technol.* **2013**, *2*, P76−P80.
(23) Ouyang, S.; Li, Z.; Ouyang, Z.; Yu, T.; Ye, J.; Zou, Z. *J. Phys. Chem. C* **2008**, *112*, 3134−3141.
(24) Ouyang, S.; Ye, J. *J. Am. Chem. Soc.* **2011**, *133*, 7757−63.
(25) Banerjee, A. N.; Maity, R.; Chattopadhyay, K. K. *Mater. Lett.* **2003**, *58*, 10−13.
(26) Reddy, A. S.; Park, H.-H.; Rao, G. M.; Uthanna, S.; Reddy, P. S. *J. Alloys. Compd.* **2009**, *474*, 401−405.
(27) Götzendörfer, S.; Polenzky, C.; Ulrich, S.; Löbmann, P. *Thin Solid Films* **2009**, *518*, 1153−1156.

(28) Bywalez, R.; Götzendörfer, S.; Löbmann, P. *J. Mater. Chem.* **2010**, *20*, 6562.
(29) Li, D.; Fang, X.; Deng, Z.; Zhou, S.; Tao, R.; Dong, W.; Wang, T.; Zhao, Y.; Meng, G.; Zhu, X. *J. Phys. D: Appl. Phys.* **2007**, *40*, 4910−4915.
(30) Neumann-Spallart, M.; Pinto, R. *Thin Solid Films* **2011**, *520*, 1299−1302.
(31) Ouyang, S.; Kikugawa, N.; Chen, D.; Zou, Z.; Ye, J. *J. Phys. Chem. C* **2009**, *113*, 1560−1566.
(32) Nagarajan, R.; Duan, N.; Jayaraj, M. K.; Li, J.; Vanaja, K. A.; Yokochi, A.; Draeseke, A.; Tate, J.; Sleight, A. W. *Int. J. Inorg. Mater.* **2001**, *3*, 265−270.
(33) Kumar, S.; Miclau, M.; Martin, C. *Chem. Mater.* **2013**, *25*, 2083−2088.
(34) Sato, T.; Sue, K.; Tsumatori, H.; Suzuki, M.; Tanaka, S.; Kawai-Nakamura, A.; Saitoh, K.; Aida, K.; Hiaki, T. *J. Supercrit. Fluids* **2008**, *46*, 173−177.
(35) Zhou, S.; Fang, X.; Deng, Z.; Li, D.; Dong, W.; Tao, R.; Meng, G.; Wang, T.; Zhu, X. *J. Cryst. Growth* **2008**, *310*, 5375−5379.
(36) Saha, B.; Thapa, R.; Chattopadhyay, K. K. *Mater. Lett.* **2009**, *63*, 394−396.
(37) Kumekawa, Y.; Hirai, M.; Kobayashi, Y.; Endoh, S.; Oikawa, E.; Hashimoto, T. *J. Therm. Anal. Calorim.* **2010**, *99*, 57−63.
(38) Ahmed, J.; Blakely, C. K.; Prakash, J.; Bruno, S. R.; Yu, M.; Wu, Y.; Poltavets, V. V. *J. Alloys. Compd.* **2014**, *591*, 275−279.
(39) Amrute, A. P.; Łodziana, Z.; Mondelli, C.; Krumeich, F.; Pérez-Ramírez, J. *Chem. Mater.* **2013**, *25*, 4423−4435.
(40) Banerjee, A. N.; Chattopadhyay, K. K. *J. Appl. Phys.* **2005**, *97*, 084308.
(41) Shahriari, D. Y.; Barnabè, A.; Mason, T. O.; Poeppelmeier, K. R. *Inorg. Chem.* **2001**, *40*, 5734−5735.